World Academy of Science, Engineering and Technology
International Journal of Aerospace and Mechanical Engineering
Vol:18, No:3, 2024

Hydrogen-Fueled Micro-Thermophotovoltaic Power Generator: Flame Regimes and Flame Stability

Hosein Faramarzpour

***Abstract*—**This work presents the optimum operational conditions for a hydrogen-based micro-scale power source, using a verified mathematical model including fluid dynamics and reaction kinetics. Thereafter, the stable operational flame regime is pursued as a key factor in optimizing the design of micro-combustors. The results show that with increasing velocities, four H_2 flame regimes develop in the micro-combustor, namely: 1) periodic ignition-extinction regime, 2) steady symmetric regime, 3) pulsating asymmetric regime, and 4) steady asymmetric regime. The first regime that appears in 0.8 m/s inlet velocity is a periodic ignition-extinction regime which is characterized by counter flows and tulip-shape flames. For flow velocity above 0.2 m/s, the flame shifts downstream, and the combustion regime switches to a steady symmetric flame where temperature increases considerably due to the increased rate of incoming energy. Further elevation in flow velocity up to 1 m/s leads to the pulsating asymmetric flame formation, which is associated with pulses in various flame properties such as temperature and species concentration. Further elevation in flow velocity up to 1 m/s leads to the pulsating asymmetric flame formation, which is associated with pulses in various flame properties such as temperature and species concentration. Ultimately, when the inlet velocity reached 1.2 m/s, the last regime was observed, and a steady asymmetric regime appeared.

***Keywords*—**Thermophotovoltaic generator, micro combustor, micro power generator, combustion regimes, flame dynamic.

I. Introduction

UTILIZATION of micro-thermophotovoltaic generators is a solution for micro-scale power generation or "power Micro-Electromechanical System (MEMS)". High power density of micro-thermophotovoltaic generators compared to advanced batteries makes micro-thermophotovoltaic generators as a feasible technology for miniaturized power generation [1]. In addition, thermophotovoltaic generators offer fuel flexibility, portability, reliability and 24-hour usability. Operation of thermo-photovoltaic generator is based on utilizing the radiative heat emitted from heated surfaces with temperatures above 800 °C [2]. Another important feature of thermophotovoltaic generators is their potential for simultaneous utilization with various generator types [3], [4]. This feature becomes important when the exhaust gases contain high temperature and consequently high outgoing energy. An example of simultaneous utilization of thermophotovoltaic with other power generators is given by Qiu and Hayden [5] where they proposed simultaneous utilization of thermophotovoltaic and thermo-electric generators reaching a higher efficiency than using each generator alone. The power law dependence of radiation on temperature, following the Boltzmann law, implies that even moderate increases in temperature can significantly enhance efficiency. According to Qiu and Hayden [5] if the generator inlet temperature increases from 25 °C to 550 °C, the efficiency increases from 12-14% to 19%. Another merit associated with thermophotovoltaic modules is that their efficiency increases with module size reduction. For instance, size reduction for thermophotovoltaic generators of Paul Scherrer Institute (PSI) from 20 kW to 2 kW led to doubling the efficiency [2]. There are considerable efforts in increasing thermophotovoltaic efficiency by improving combustion efficiency, increasing temperature and size reduction. Obviously, other factors such as inlet properties (fuel type, flow velocity and equivalence ratio) and combustor geometry also affect thermophotovoltaic efficiency.

To achieve an enhanced efficiency in micro-thermophotovoltaic power generators via temperature enhancement, combustion in micro-combustors should be modified in a way that the highest possible temperature is obtained. Hydrogen (H_2) as a clean carbon-free fuel has one of the highest flame temperatures which can make H_2 as the key alternative to hydrocarbon fuels. In addition to high flame temperature, H_2 has high diffusivity, high reaction rate, and high flame velocity. However, H_2 raises some concerns in the industry regarding flame instability, laminar flame velocity, diffusion coefficients, and flammability limit in micro-combustors.

Identifying the stable operational flame regimes is key to optimize the design of micro-combustors [6]. The small size of micro-combustors leads to enhanced interaction between the walls and the flame leading to new combustion regimes compared to large combustion chambers [7], [8]. Generally, micro combustors are associated with low Reynolds number due to the low flow velocities and relatively modest length scales leading to the increased share of diffusion from total mass transport within the reactor. Pizza et al. [9] used a 2-dimensional direct numerical simulation (DNS) method to investigate the effects of the inlet velocity and the combustor diameter on flame dynamics in a micro combustor. They found that the initial flame follows an ignition/extinction regime. When they increased the flow velocity the flame regime changed to the mild combustion, periodic ignition/extinction, closed symmetric stable flames, open symmetric stable flames, oscillating flames, and asymmetric stable flames. Akram and Kumar [10] studied H_2-air flame dynamics in a diverging

H. F. is with the Department of Mechanical Engineering, Université de Sherbrooke, Sherbrooke, Québec, Canada, J1K 2R1 (e-mail: Hosein.Faramarzpour@usherbrooke.ca).

channel focusing on flow velocity and channel divergence angle reporting combustion regimes of planar flame, negatively stretched flame, positively stretched flame, partially stable flame, stable flame, symmetric flame, partially stable regime, and asymmetric flame. They reported planar flame close to flashback limit in the fuel-rich flame. When the speed increases, the flame became stretched with convex shape in both symmetric and un-symmetric regimes. Yamamoto et al. [11] studied the stoichiometric combustion of Heptane-air with temperature gradient in a micro combustor. They reported three regimes of symmetric steady regime at high speeds, ignition-extinction regime at medium speeds, and weak steady regime, weak transparent regime and stretched transparent regime at low speeds. Nakamura et al. [12] used a one-dimensional numerical approach to study the ignition-extinction instability of methane-air mixture and they concluded that the ignition-extinction regime occurs in two stages due to the presence of intermediate radicals such as CO and CH_2. It means that the flame initially converts the CH_4 molecules to either final combustion products or intermediate components and then the intermediate components such as CH_2 and CO generate two flame branches. Fan et al. [13] experimentally investigated the H_2-air flames in a micro combustor and reported fluctuating regimes with changing equivalence ratio, velocity and wall temperature gradients. They found that the local extinction in flame front leads to a moving flame and then to separation into two flames. In addition, they reported that the circular unsteady flame was generated due to flame separation and found that the flame extinction close to the walls was in spiral forms at high inlet flow velocities. In another study, Brambilla et al. [14] using CO-H_2-air flame, found four combustion regimes keeping equivalence ratio and the CO/O_2 ratio constant. After the periods with no ignition, pulsating ignition associated with hot spots from strong combustion appears leading to a weak flame. The unsteady weak flame changes to a strong V-shape flame due to frequent ignitions at multiple locations close to the walls at temperatures above 1000 K. Kamada et al. [15] investigated the natural gas flame (methane, ethane, and butane) and mixture of methane and butane in a micro burner with a weak flame at various locations. They found that addition of butane to the mixture reduces the flame temperature and moves the flame more toward the entrance. Ethane in their study had the minimum flame temperature and closest flame to the entrance. As seen in the above studies, there are various publications regarding the micro combustor regimes using various fuels. However, a knowledge gap can be seen when it comes to increasing thermophotovoltaic efficiencies using H_2–fired micro combustors.

This study explores various flame regimes in micro-combustor as a heat source for a micro-thermophotovoltaic generator and micro-gas turbine. The aims of this work are to 1) present the properties of H_2 flame regimes at varying operational conditions of a micro-thermophotovoltaic power generator, 2) suggest the optimum flame regime for achieving highest efficiency in a thermophotovoltaic module and showing the associated measured outer wall temperature.

II. Numerical Approach

The mathematical model covers coupled Navier-Stokes equations, energy conservation equation, species conservation equations and combustion reaction equations. Crank-Nicholson approach is utilized to meet the Courant–Friedrichs–Lewy (CFL) stability condition of explicit schemes. Pressure-Implicit with Splitting of Operators (PISO) approach is chosen for the coupling pressure and velocity. Since this work deals with low Mach number flows, pressure term is divided to thermodynamic and hydraulic terms where thermodynamic pressure term in ambient conditions equals to atmospheric pressure and the hydraulic term depends on the momentum equation terms. The thermodynamic pressure is used in energy equation and ideal gas equation and the hydraulic term is used in momentum equation. The changes in thermodynamic properties such as the gas density due to temperature variations in the combustor are calculated according to [16]. The momentum equation is written as:

$$\rho\left(\frac{\partial u}{\partial t} + u \cdot \nabla u\right) = -\nabla p_{i1} + \nabla \cdot (\mu S) \tag{1}$$

where ρ, p_1, u and η are density, hydraulic pressure, velocity vector and dynamic viscosity respectively. The stress tensor (S) is $\nabla u + (\nabla u)^T - \frac{2}{3}(\nabla . u)I$ where I is unit vector. The equation for energy conservation is written as:

$$\rho c_p\left(\frac{\partial T}{\partial t} + u \cdot \nabla T\right) = \nabla \cdot (\lambda \nabla T) - \sum_{i=1}^{N} h_i \dot{\omega}_i - \rho\left(\sum_{i=1}^{N} c_{p,i} Y_i V_i\right) \cdot \nabla T \tag{2}$$

where λ is conductive heat transfer coefficient, C_p is the specific heat and h is the enthalpy and i is the specie i. The three terms in the right-hand side of (2) are conductive heat transfer, released energy due to the reactions and diffusive heat transfer. The ideal gas law is written as:

$$p_0 = \rho \frac{R}{\overline{W}} T \tag{3}$$

where $\overline{W}$ is average molecular weight and R is gas constant.

Since the flow in micro combustor applications has low velocity and the flow lies in laminar regime, molecular diffusion becomes of particular importance. It should be noted that the mixing, either convective or diffusive, has key role in reactor efficiencies [17], [18]. The mass conservation equation for N species considering diffusion is written as (4) where two right hand side terms refer to molecular diffusing flux and the rate of consumption/generation of i^{th} specie per unit volume:

$$\rho\left(\frac{\partial Y_i}{\partial t} + u \cdot \nabla Y_i\right) = -\nabla \cdot (\rho Y_i V_i) + \dot{\omega}_i \qquad i = 1, \ldots, N \tag{4}$$

where V_i is diffusion velocity of i^{th} specie calculated as: below:

$$V_i = V_i^* + V_c \tag{5}$$

V_i^* is obtained from the kinetic theory of gases by considering only mixture averaged diffusion. V_c is defined as the correction velocity to numerically guarantee total mass conservation [19]

where V_i^* and V_c is calculated as:

$$V_c = -\sum_{i=1}^{N_g} Y_i V_i^* \quad (6)$$

$$V_i* = -D_{im} X_i \nabla X_i \quad (7)$$

D_{im} is molecular dispersion coefficient and X_i is the molar concentration. D_{im} is calculated as blow:

$$D_{im} = \frac{1-x_i}{\sum_{j\neq i}(\frac{x_j}{D_{ij}})} \quad (8)$$

where D_{ij} is molecular dispersion coefficient of specie i in specie j calculated according to Chapman-Enskog equation as [20]:

$$D_{ij} = 10 \cdot 1325 \frac{0.001858\, T^{1.5} (W_{ij})^{-0.5}}{p\, \sigma_{ij}^2 \Omega_D} \quad (9)$$

$$\sigma_{ij} = \frac{\sigma_i + \sigma_j}{2} \quad (10)$$

$$W_{ij} = (\frac{1}{W_i} + \frac{1}{W_j})^{-1} \quad (11)$$

$$\Omega_D = \frac{1.06036}{T_N^{0.15610}} + \frac{0.193}{\exp(0.47635\, T_N)} + \frac{1.03587}{\exp(1.52996\, T_N)} + \frac{1.76474}{\exp(3.89411\, T_N)} \quad (12)$$

$$T_N = \frac{T}{E_{ij}} \quad (13)$$

$$E_{ij} = \varepsilon_{ij}/k_B \quad (14)$$

$$\varepsilon_{ij} = (\sqrt{\varepsilon_i \varepsilon_j}) \quad (15)$$

where W is molecular mass, σ is impact diameter, KB is Boltzmann constant, ε_α is the Lenard-Jones energy parameter and subscript i refers to specie i.

Heating the outer wall of the micro combustor has been a good approach to stabilize the flame, both in modeling and in experimental methods. Heating the wall can be performed using a heater leads to a temperature gradient on the wall. The wall temperature gradient is defined as (16) where the temperature changes from 300 K to 960 K.

$$T_w = 300 + 660 \tanh \frac{x}{l/20} \quad (16)$$

In this research, detailed chemical kinetics including nine species and 21 reactions are used for hydrogen/air mixture according to reaction mechanism proposed by Pizza et al. [9], [21], [22].

III. Validation and Grid Independence

Fig. 1 shows combustor maximum temperature at various mesh sizes. As can be seen, the temperature for 37500 meshes is similar to the larger mesh numbers indicating that the results reach grid independence for 37500 mesh numbers. Additional cell size condition is proposed by Poinsot and Veynanye [23] that having 15 cells in the flame front is necessary. Thus, the flame front size is approximated using the approach given in [23]. The cell size chosen in this work is 25 μm×25 μm, which satisfies both conditions stated above regarding grid independence and having 15 cells in the flame front.

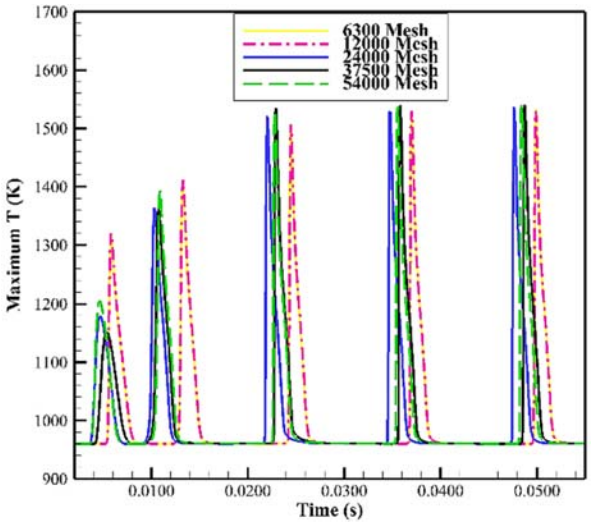

Fig. 1 Maximum temperature at various mesh sizes

Fig. 2 shows the maximum combustor temperature in ignition-extinction regime of this wok compared to the work by Pizza et al. [9]. The results in Fig. 2 show that the modeling of this work agrees well with Pizza et al. [9], and that it can follow the ignition-extinction trends properly. In addition, the duration of the pulses and the value of the maximum temperature agree well with [9]. The temperature variations can help calculating the properties of flame pulses and wave generations.

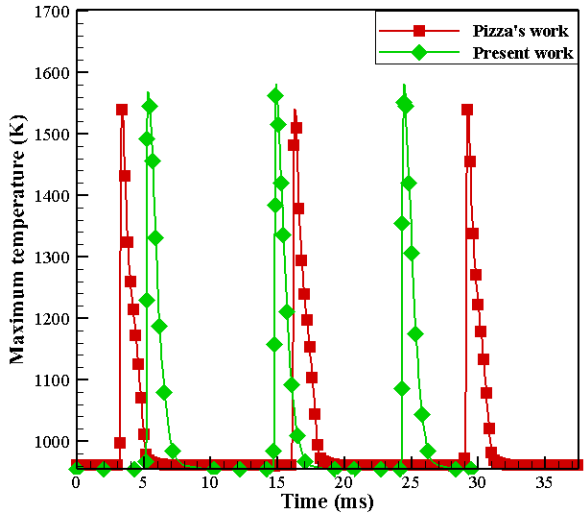

Fig. 2 Maximum combustor temperature in ignition-extinction regime of this wok compared to the work by Pizza et al. [9]

Fig. 3 gives the comparison of modeled temperature profile inside the combustor with experimental results of Toro et al. [24], showing a good agreement between the modeling of this work and the experimental in-situ temperature profile.

As seen in the validation figures the developed code predict

almost accurately the NO_x emission and mean wall temperature.

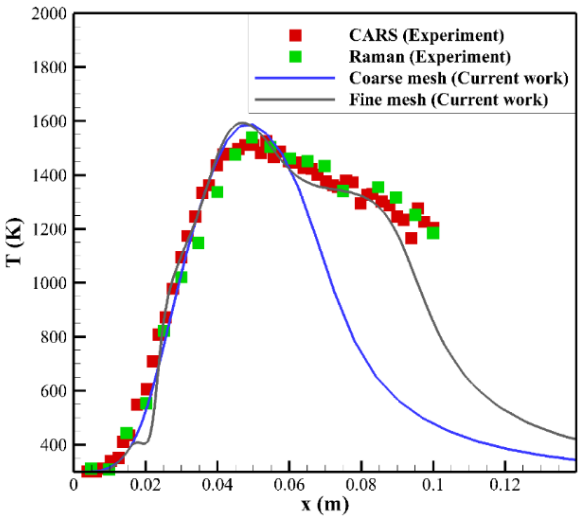

Fig. 3 Comparison of modeled temperature profile inside the combustor with experimental results of [24]; CARS refers to "coherent anti-Stokes Raman scattering" method and Raman refers to "spontaneous Raman scattering" method

IV. Results and Discussion

A. Periodic Ignition-Extinction Regime

Fig. 4 shows the contour of OH mass concentration at various time steps. What can be described from the trends in Fig. 4 is a periodic ignition-extinction regime initiating from wall vicinities and then approaching the center. With the increase in time the circle-shape flame is stretched and divided to two parts where the forward part goes to the unburned gases close to exhaust and after consuming the unburned gases extinct. The backward part of the flame goes toward the cold incoming gases which reduces the flame propagation rate. This trend in flame propagation is similar to the flameless combustion.

It should be noted that the periodic ignition-extinction regime is reported in velocities of 0.04 m/s < u < 0.18 m/s by Pizza et al. [9], 0.3 m/s by Norton et al. [25] in methane-air mixture and 0.08 m/s < u < 0.16 m/s by this work. So, while the upper limit of the periodic ignition-extinction is similar between this work and Pizza et al. [9], the velocity where periodic ignition-extinction regime starts is different which might be due to the presence of physical perturbations in Pizza et al. [9] leading to approach this regime faster.

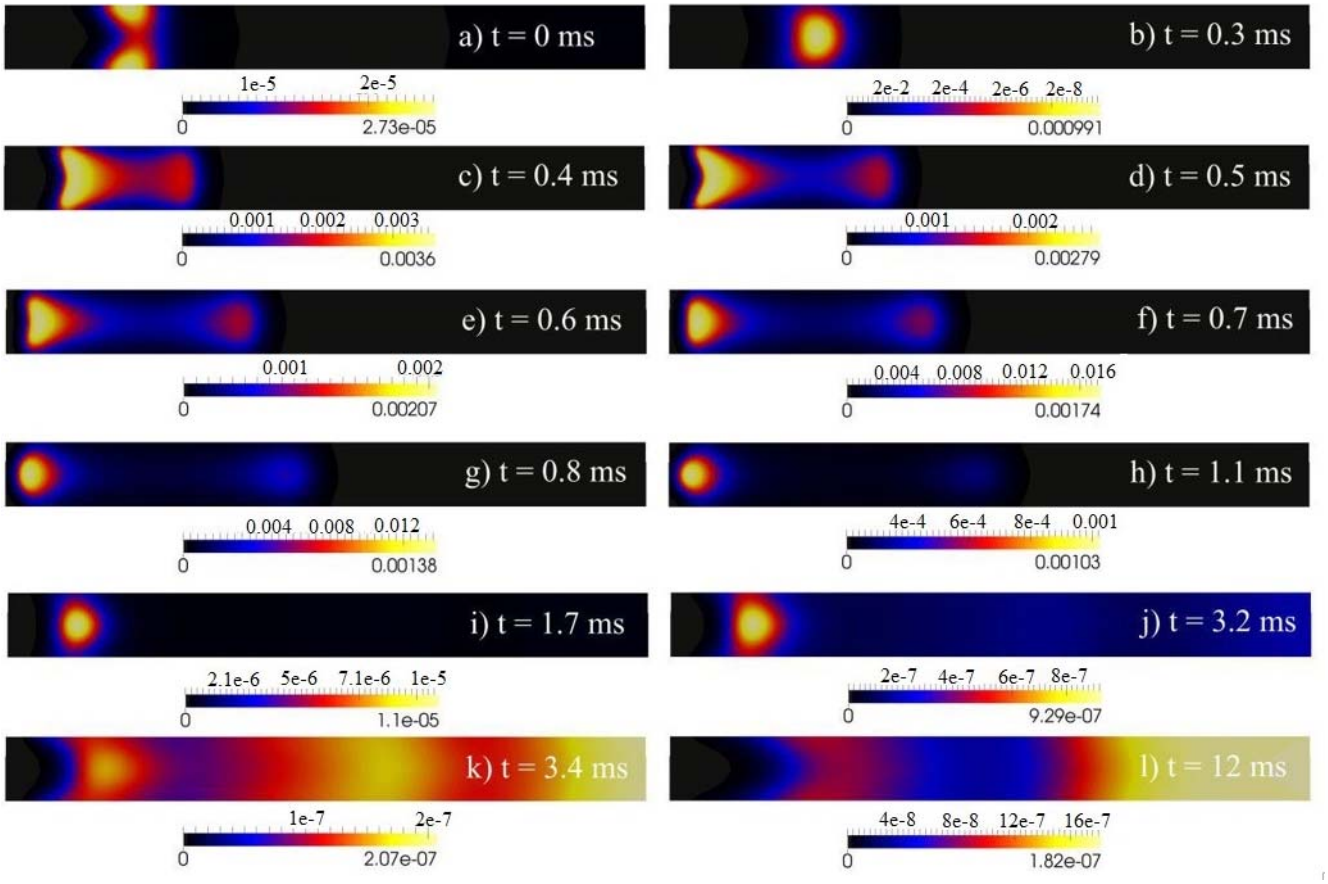

Fig. 4 The contour of OH mass concentration at various time steps at velocity inlet of 0.1 m/s

Fig. 5 shows the generation rate of OH radicals at various time steps. As seen, the flame initiated at 0.3 ms and after 0.1 ms separated and departed toward the exit. Two peaks after 0.3 ms shows the movement of the flame toward both sides of the

combustor. This figure shows a proper view of the generation and motion of the flame.

Fig. 6 shows the rate of energy release with two peaks and two consumption points for H_2 consumption. The periodic ignition-extinction regime can be divided to three stages of initiation, ignition and propagation. Fig. 6 shows the propagation stage where H_2 and O_2 are reactants and OH and H_2O are combustion products. Two peaks are observed showing flame fronts in positive and negative directions. Surprisingly, the H_2 and O_2 which are reactants are still present in post combustion showing the importance of enough residence time to allow the remaining reactants burn in what can be expected to be a diffusion flame. Temperature can also be seen to have its peak between two species peaks.

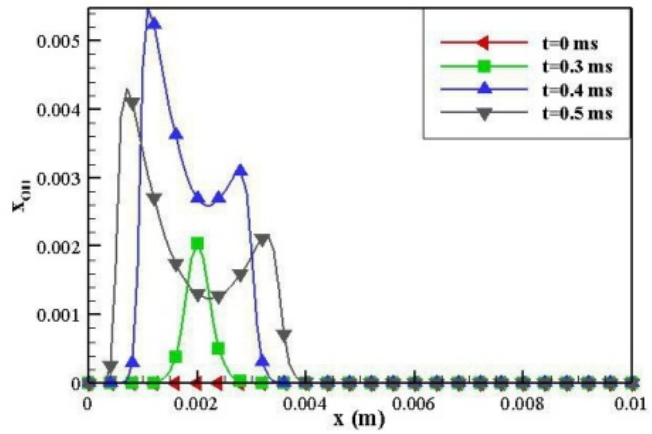

Fig. 5 The generation rate of OH at various times

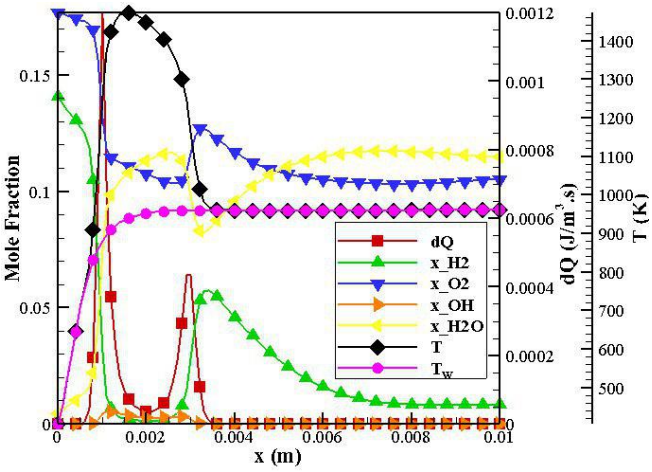

Fig. 6 The rate of species generation and energy release at t = 0.4 ms

Fig. 7 shows the temperature profile at the centerline of the combustor. With the initiated flame, temperature increases and moves to both sides of the combustor. For instance, at t = 0.8 ms two peaks can be detected showing two flame fronts moving to both ends. The peaks have different temperatures due to varying radical concentration in exhaust side and in entrance side. At higher times, the flame in both sides is going toward extinction and the temperature approaches the wall temperature.

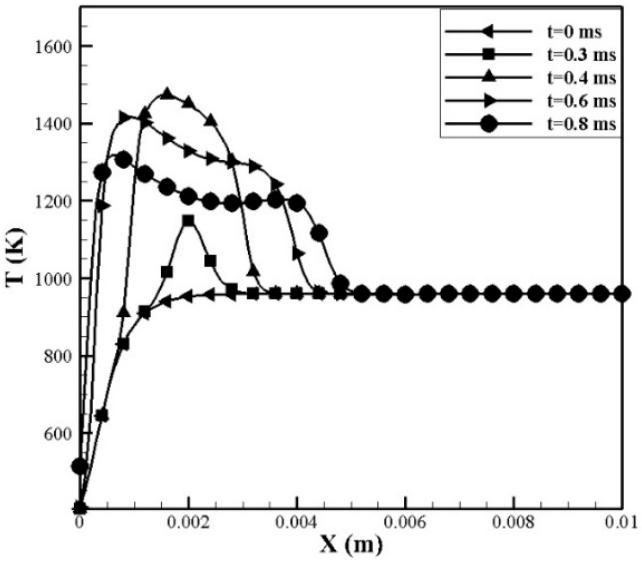

Fig. 7 Temperature profile in the centerline of the combustor at inlet velocity of 0.1 m/s and equivalence ratio of 0.5

B. Steady Symmetric Regime

When the flow velocity increases above 0.2 m/s, the combustion regime changes to a steady symmetry regime. The symmetry line in this case is the centerline of the combustor. The maximum concentration of OH radicals and also temperature in steady symmetric regime are located at the center line.

Figs. 8 and 9 show the contours of OH radical concentrations and temperature in steady symmetric regime at inlet velocity of 0.75 m/s. As seen, the flame is moving away from the combustor entrance and changes the shape from convex to concave. At low velocities, the flame is convex toward the reactants. With increasing velocity of incoming gases, the flame at the center faces instability problems and thus the flame approaches the walls where the stability is more achievable making the flame shape as concave. At flow velocities above 0.7 m/s the flame is fully concave.

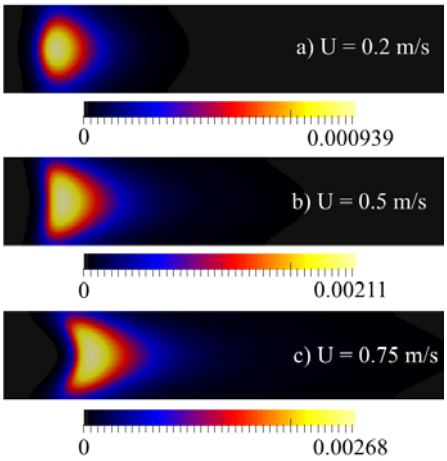

Fig. 8 OH radical contour in a steady symmetric flame at equivalence ratio of 0.5

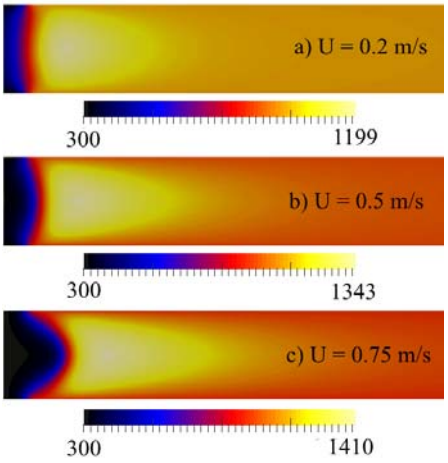

Fig. 9 Temperature contour in a steady symmetric flame at equivalence ratio of 0.5

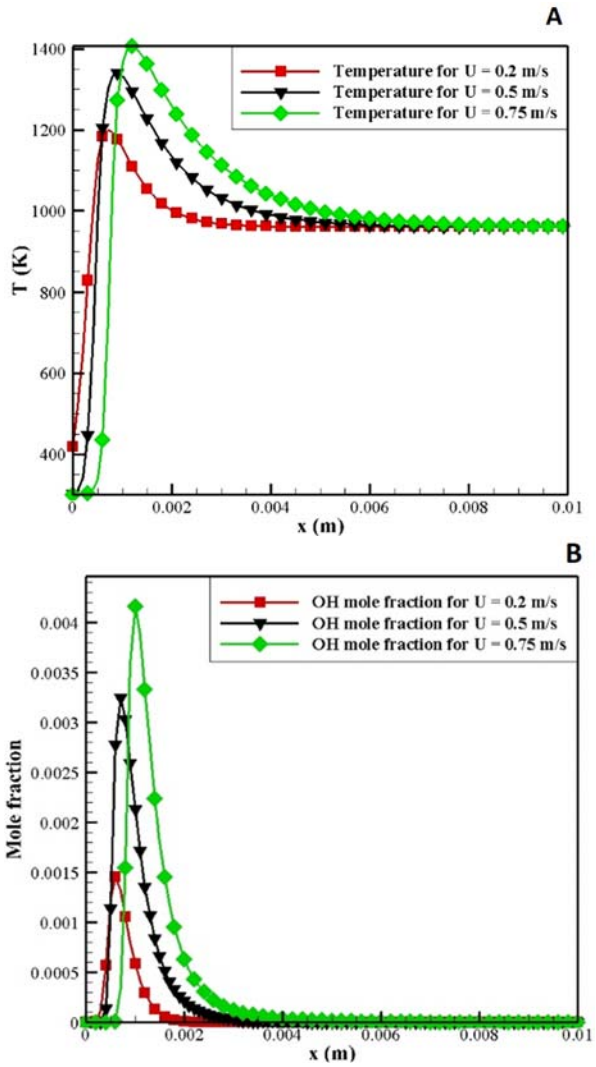

Fig. 10 The profiles of (a) temperature and (b) OH radicals in steady symmetric regime at equivalence ratio of 0.5

Fig. 10 shows the profiles of OH radical concentration and temperature for three velocities of 0.2, 0.5 and 0.75 m/s. The flame moves toward the exit with the increase in the velocity while the temperature increases due to the increased incoming energy flux. The temperature increase is more evident at velocities of 0.2 and 0.5 m/s.

C. Oscillating Asymmetric Flame

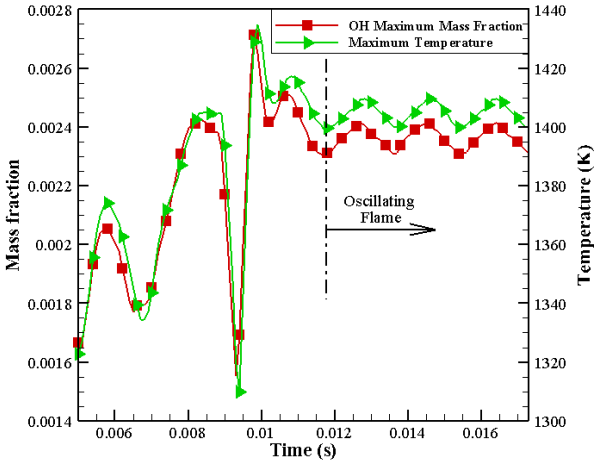

Fig. 11 OH mass fraction and temperature profile in a pulsating asymmetric flame at inlet velocity of 0.1 m/s and equivalence ratio of 0.5

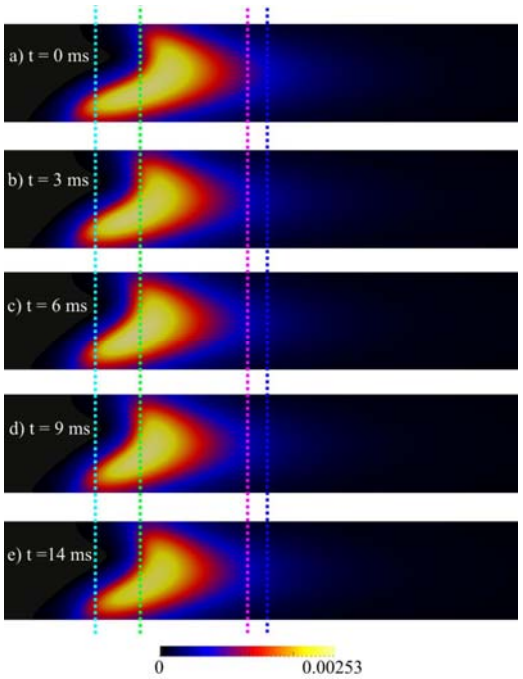

Fig. 12 Contour of OH radicals in the micro combustor in pulsating asymmetric regime

At velocities of 1 m/s, the flame mode changes to pulsating asymmetric. This regime is also reported by Pizza et al. [9] describing its asymmetry as its main feature. This work shows the pulsating nature of this regime in Fig. 11. Fig. 12 shows the OH mass concentration and temperature inside the micro combustor in pulsating asymmetric regime. As seen after 0.01 s, the flame shows a pulsating behavior where OH

concentration pulsations represent the periodic behavior of species and temperature pulses show the flame periodic or pulsating behavior.

D.Asymmetric Steady Flame

When the flow velocity increases further, the pulsating asymmetric regime reaches a stable condition and the combustion regime changes to a steady asymmetric regime. In a specific flow velocity in steady asymmetric regime, the flame can have two configurations with the same probability. Depending on angle above or below 90, the flow can be located above or below centerline with the name of a top asymmetric flame or bottom asymmetric flame.

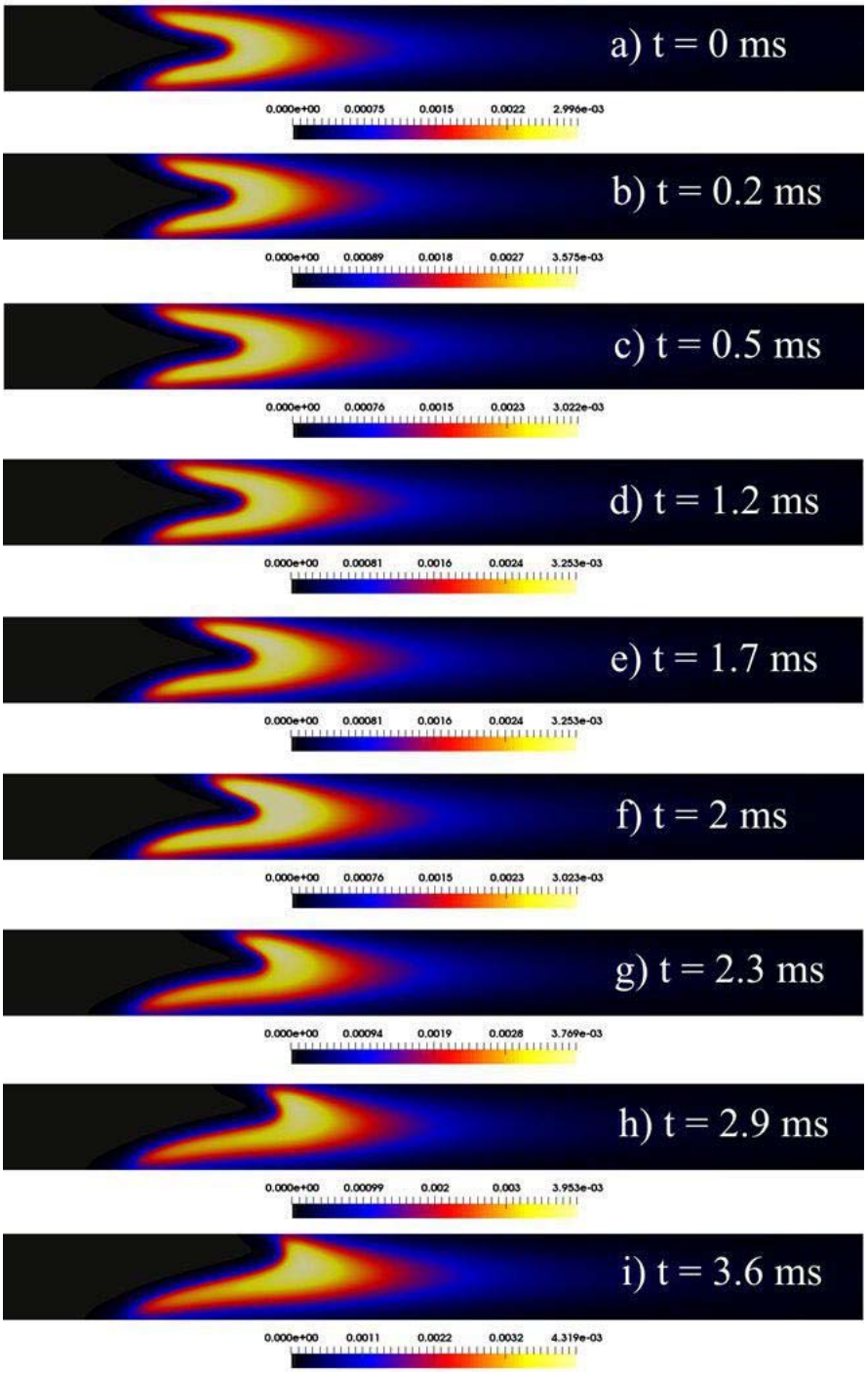

Fig. 13 Contour of temperature in a steady asymmetric regime

Figs. 13 and 14 show the contours of temperature and OH radical, respectively, in steady asymmetric regime. As shown in Fig. 13, the flame initiated in symmetric form but gradually changes to an asymmetric flame type. Fig. 14 shows both top

and bottom asymmetric flame. The occurrence of each of these two modes depends on the initial conditions and disturbances. The main reason for such asymmetric flames is hydrodynamic instabilities at relatively high micro combustor velocities and thermal-diffusive instabilities. For instance, high velocities lead to diffusion of light and highly reactive radicals such as H and O from centerline toward the walls and consequently formation of asymmetry in the flame. Our results on the steady asymmetric flame are in agreement with the findings of Pizza et al. [9].

E. Lewis Number (Le)-Dependence of Asymmetries

The instabilities that cause the asymmetry in the flame are formed by various physical phenomena such as thermal and mass diffusion instabilities. Lewis number is a measure for assessing the ratio of thermal diffusivity to mass diffusivity and can be used to quantitatively evaluate the asymmetries and diffusive-thermal instability in the flame.

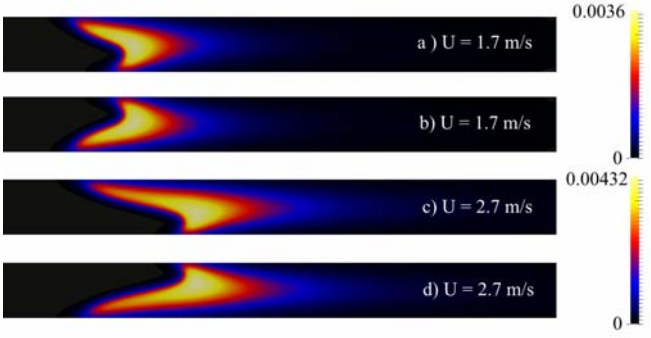

Fig. 14 Contour of OH radicals in a steady asymmetric regime

Fig. 15 shows the contours of OH, H and T for Le numbers of one and 0.4, respectively, at inlet velocity of 2.7 m/s and equivalence ratio of 0.5. As seen, changing the Le leads to formation of asymmetry in the flame, which shows that the thermal-mass diffusion mechanism is behind the asymmetry generation.

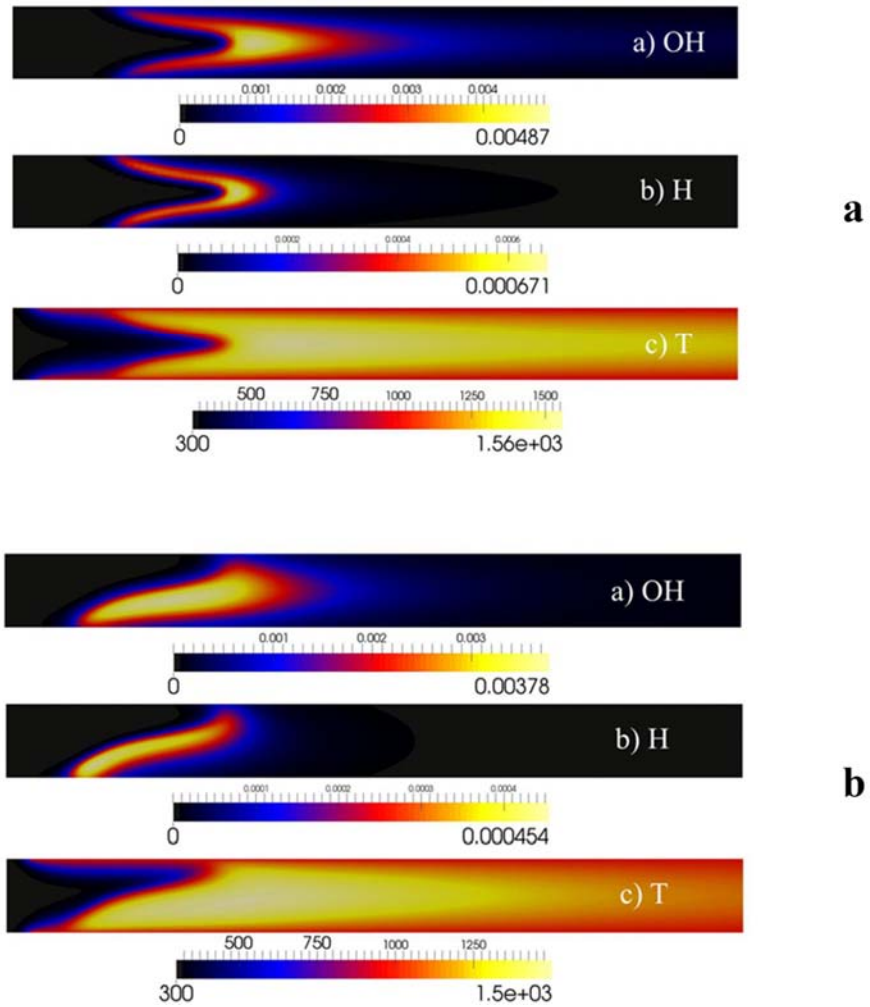

Fig. 15 The contours of OH, H and T for Le numbers of 1: (a) and 0.4 (b) at the inlet velocity of 2.7 m/s and equivalence ratio of 0.5

Fig. 16 (a) shows the Le number for specie H at the centerline of the micro combustor for various inlet velocities at equivalence ration of 0.5 and Fig. 16 (b) represents the relevant contour of the Le number. The Le number increases in the

combustor and then drops when reaching the flame zone. This drop in the Le number is considerably larger in high velocities compared to low velocities. The large drop in the Le number at high velocity shows the transition from symmetric flame to asymmetric flame.

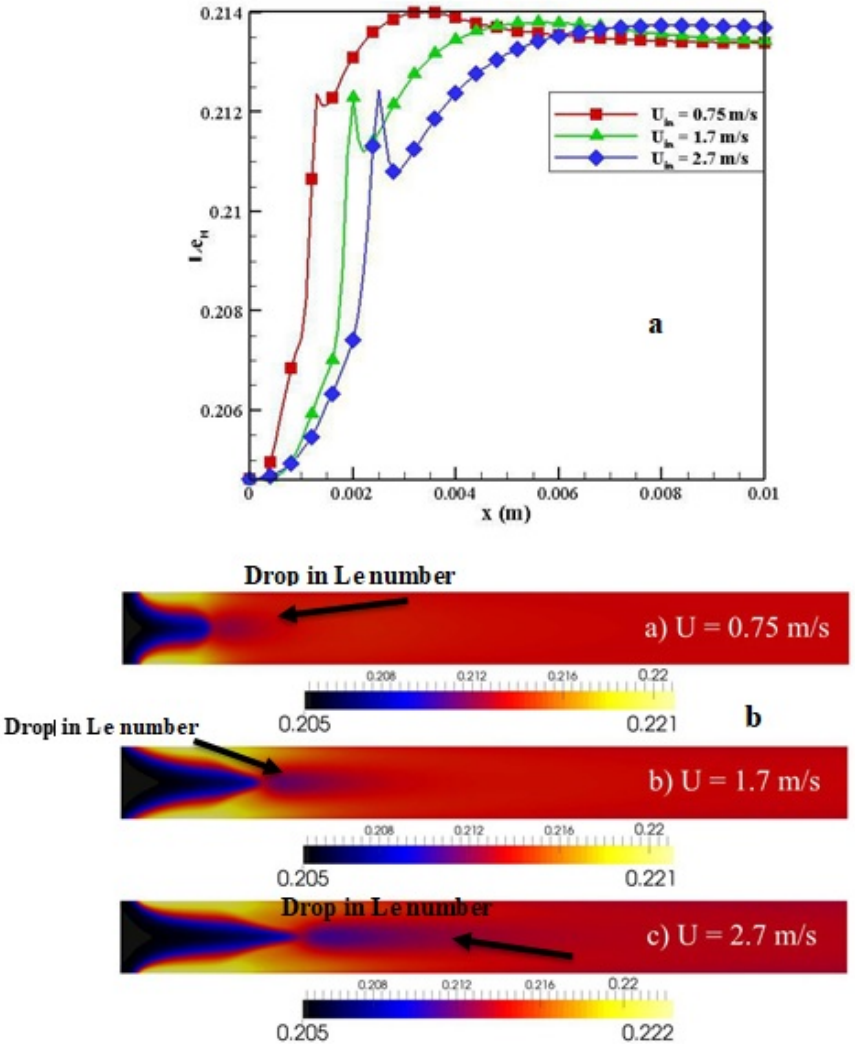

Fig. 16 (a) Le number in centerline of combustion chamber and (b) contour of Le number

V. Conclusion

In this work, the H_2 flame is investigated using a mathematical model which is developed for simulation of H_2-air combustion in micro combustors considering both fluid dynamics and reaction kinetics. The modeling results show that with increasing velocities four regimes are observed namely: 1) periodic ignition-extinction regime, 2) steady symmetric regime, 3) pulsating asymmetric regime, and 4) steady asymmetric regime. The main features of the periodic ignition-extinction regime are counter flows and tulip-shape flames. With increase in flow velocity, the flame location moves downstream and the combustion regime changes to steady symmetric flame. In steady symmetric flame, the combustor temperature increases considerably due to the increased rate of incoming energy. With further increase in flow velocity the pulsating asymmetric flame forms, which is associated with flame location changes and pulses in all flame properties such as temperature and species concentration. The final regime observed with highest velocities in this work is asymmetric steady flame which the location of flame can show two modes of top asymmetric flame or bottom asymmetric flame. Increases in flow velocity increases the asymmetry and elongates the flame, making it narrower. The mode of the steady asymmetric flame depends on the properties of hydrodynamic instability or thermal-diffusive instability which first causes deviation from the symmetric flame.

References

[1] J. Li, Q. Li, Y. Wang, Z. Guo, X. Liu, Fundamental flame characteristics of premixed H2–air combustion in a planar porous micro-combustor, Chemical engineering journal 283 (2016) 1187-1196.

[2] H. Daneshvar, R. Prinja, N.P. Kherani, Thermophotovoltaics: Fundamentals, challenges and prospects, Applied Energy 159 (2015) 560-575.

[3] M. Bianchi, C. Ferrari, F. Melino, A. Peretto, Feasibility study of a Thermo-Photo-Voltaic system for CHP application in residential

buildings, Applied Energy 97 (2012) 704-713.
[4] E.S. Barbieri, P.R. Spina, M. Venturini, Analysis of innovative micro-CHP systems to meet household energy demands, Applied Energy 97 (2012) 723-733.
[5] K. Qiu, A. Hayden, Increasing the efficiency of radiant burners by using polymer membranes, Applied Energy 86(3) (2009) 349-354.
[6] M. Malushte, S. Kumar, Flame dynamics in a stepped micro-combustor for non-adiabatic wall conditions, Thermal Science and Engineering Progress 13 (2019) 100394.
[7] Y. Ju, B. Xu, Theoretical and experimental studies on mesoscale flame propagation and extinction, Proceedings of the Combustion Institute 30(2) (2005) 2445-2453.
[8] K. Maruta, T. Kataoka, N.I. Kim, S. Minaev, R. Fursenko, Characteristics of combustion in a narrow channel with a temperature gradient, Proceedings of the combustion institute 30(2) (2005) 2429-2436.
[9] G. Pizza, C.E. Frouzakis, J. Mantzaras, A.G. Tomboulides, K. Boulouchos, Dynamics of premixed hydrogen/air flames in mesoscale channels, Combustion and Flame 155(1-2) (2008) 2-20.
[10] M. Akram, S. Kumar, Experimental studies on dynamics of methane–air premixed flame in meso-scale diverging channels, Combustion and flame 158(5) (2011) 915-924.
[11] A. Yamamoto, H. Oshibe, H. Nakamura, T. Tezuka, S. Hasegawa, K. Maruta, Stabilized three-stage oxidation of gaseous n-heptane/air mixture in a micro flow reactor with a controlled temperature profile, Proceedings of the Combustion Institute 33(2) (2011) 3259-3266.
[12] H. Nakamura, A. Fan, S. Minaev, E. Sereshchenko, R. Fursenko, Y. Tsuboi, K. Maruta, Bifurcations and negative propagation speeds of methane/air premixed flames with repetitive extinction and ignition in a heated microchannel, Combustion and Flame 159(4) (2012) 1631-1643.
[13] A. Fan, S. Minaev, E. Sereshchenko, Y. Tsuboi, H. Oshibe, H. Nakamura, K. Maruta, Dynamic behavior of splitting flames in a heated channel, Combustion, Explosion, and Shock Waves 45 (2009) 245-250.
[14] A. Brambilla, C.E. Frouzakis, J. Mantzaras, A. Tomboulides, S. Kerkemeier, K. Boulouchos, Detailed transient numerical simulation of H2/air hetero-/homogeneous combustion in platinum-coated channels with conjugate heat transfer, Combustion and Flame 161(10) (2014) 2692-2707.
[15] T. Kamada, H. Nakamura, T. Tezuka, S. Hasegawa, K. Maruta, Study on combustion and ignition characteristics of natural gas components in a micro flow reactor with a controlled temperature profile, Combustion and Flame 161(1) (2014) 37-48.
[16] A. Majda, J. Sethian, The derivation and numerical solution of the equations for zero Mach number combustion, Combustion science and technology 42(3-4) (1985) 185-205.
[17] I. Bahrabadi-Jovein, S. Seddighi, J. Bashtani, Sulfur Dioxide Removal Using Hydrogen Peroxide in Sodium-and Calcium-Based Absorbers, Energy & Fuels 31(12) (2017) 14007–14017.
[18] J. Bashtani, S. Seddighi, I. Bahrabadi-Jovein, Control of nitrogen oxide formation in power generation using modified reaction kinetics and mixing, Energy 145 (2018) 567-581.
[19] A. Alipoor, K. Mazaheri, Combustion characteristics and flame bifurcation in repetitive extinction-ignition dynamics for premixed hydrogen-air combustion in a heated micro channel, Energy 109 (2016) 650-663.
[20] S. Turns, An Introduction to Combustion: Concepts and Applications, McGraw-Hill, Mc Graw Hill2000.
[21] G. Pizza, J. Mantzaras, C.E. Frouzakis, Flame dynamics in catalytic and non-catalytic mesoscale microreactors, Catalysis Today 155(1-2) (2010) 123-130.
[22] G. Pizza, C.E. Frouzakis, J. Mantzaras, A.G. Tomboulides, K. Boulouchos, Three-dimensional simulations of premixed hydrogen/air flames in microtubes, Journal of Fluid Mechanics 658 (2010) 463-491.
[23] T. Poinsot, D. Veynante, Theoretical and numerical combustion, RT Edwards, Inc.2005.
[24] V. Toro, A. Mokhov, H. Levinsky, M. Smooke, Combined experimental and computational study of laminar, axisymmetric hydrogen–air diffusion flames, Proceedings of the Combustion Institute 30(1) (2005) 485-492.
[25] D.G. Norton, D.G. Vlachos, Combustion characteristics and flame stability at the microscale: a CFD study of premixed methane/air mixtures, Chemical engineering science 58(21) (2003) 4871-4882.